American International Journal of Research in Science, Technology, Engineering & Mathematics

Available online at http://www.iasir.net

AIJRSTEM is a refereed, indexed, peer-reviewed, multidisciplinary and open access journal published by International Association of Scientific Innovation and Research (IASIR), USA
(An Association Unifying the Sciences, Engineering, and Applied Research)

Analytical DC Model of Double Channel Dual Material Gate $Al_mGa_{1-m}N$/GaN High Electron Mobility Transistor, Ultra High Speed Device for Microwave and Radar Applications

Rahis Kumar Yadav[1], Pankaj Pathak[2], R M Mehra[3]
Department of Electronics and Communication Engineering,
School of Engineering and Technology,
Sharda University,
Plot No. 32-34, Knowledge Park III, Greater Noida, Uttar Pradesh, 201306, India

***Abstract**: We present polarization dependent charge control model for current voltage characteristics of Double Channel Dual Material Gate-AlGaN/GaN HEMT. This model demonstrates complete charge control in upper and lower channel of the device under various gate and drain bias conditions. The model device structure uses GaN material with higher breakdown voltage and polarization induced charge carrier density to achieve higher voltage and current drive capability. Model and simulation results reveal that DCDMG HEMT structure is capable of reducing short-channel effects (SCEs) more effectively as compared to the available conventional devices due to the presence of the step in the channel potential profile which effectively screen the drain potential variation in the device operation. The model accurately derives the top and bottom channels currents by using effective device threshold model for each channels based on analysis of two dimensional electron gas (2-DEG) in each channel. It is observed that work function difference of dual metal gate design is reason behind the screening effect of the drain potential variation near the drain region resulting in suppressed drain induced barrier lowering (DIBL). The model analyses current density in both the channels based on polarization induced 2-DEG density. Due to presence of bottom channel in the device, the effect of current collapse in top channel alone cannot degrade device functionality as it happens in conventional single channel AlGaN/GaN HEMT. This current collapse mainly occurs in the channel closer to the gate while bottom channel being at far distance suffers minimal current collapse hence improving overall device functionality. A good agreement between the results obtained from the model, ATLAS device simulator and published experimental data provides the validity and correctness of the proposed model.*

***Keywords**: 2DEG-two dimensional electron gas, SCE- short channel effect, DMG-Dual Material Gate, DIBL-drain induced barrier lowering.*

I. Introduction

Compound semiconductor based hetrostructure devices particularly fabricated using AlGaN/GaN material system are emerging as an important option for microwave frequencies and high power applications in advanced electronic system like radar and satelite systems operating at higher voltages. Lot of research work already carried out on AlGaAs/GaAs devices for optimization and performace enhancement AlGaN/GaN High Electron Mobility Transistor (HEMT) or modulation doped field effect transistor (MODFET) are attracting considerable attention of device engineers world wide for further innovation and performance optimization. AlGaN/GaN hetrostructures devices can provide high saturation velocity, higher thermal stability at considerably higher breakdown electric field. The unique property of GaN based devices is polarization induced higher sheet charge density of 2-DEG at hetrointerface [1]. This kind of optimized hetrostructures can meet the challenges of much higher output power at higher operating voltages and power density compared with conventional AlGaAs/GaAs-HEMT [2],[3]. Long et al [4],[5] has proposed a FET structure, the dual material gate FET, in which two different metals of different workfunction were used for making dual material gate by making them contact laterally. A multi-layer structure of AlGaN/GaN double channel High Electron Mobility Transistor (DC-HEMT) was presented with detailed design, fabrication and characterisation by Chu et. al.[6] having high current gain and minimized current collapse. An analytical model of potential and electric field distribution has been developed and reported for dual channel dual material gate DCDMG-AlGaN/GaN High Electron Mobility Transistor for introduction of step functions in each channel potential profile that provides screening effects in small channel devices thus suppressing short channel effects (SCE) [19].

© 2015, AIJRSTEM All Rights Reserved

In this paper, we report a simple dc analytical model for current voltage characteristics of double channel dual material gate AlGaN/GaN HEMTs. In order to enhance the current drive capability, the efforts were made in past to fabricate AlGaN/GaN double-channel HEMTs. However, due to the additional AlGaN barrier between the two channels, accesses to the lower carrier channel were usually inefficient and double-channel behaviors were not pronounced effectively. Rongming Chu et al [6] have shown that this kind of problem can be solved by efficient design of double channel structures. Construction of an AlGaN/GaN/AlGaN/GaN multi- layer structure using a lower AlGaN barrier layer with small layer thickness and graded Al composition was proved to be an effective approach to implement the double-channel HEMT with the second channel of high electron density and acceptable access resistance. This kind of resultant AlGaN/GaN double-channel HEMT exhibit device performance better than or comparable to baseline AlGaN/GaN HEMTs in all aspects. Our DCDMG HEMT model incorporate dual material gate approach in double channel HEMT fabricated by Rongming Chu et al [6]. However, so for no analytical dc model is developed for DCDMG HEMT which incorporates benefit of dual material gate by using double channels in the single device structure.

II. Model Formulation

The schematic view of the structure of double channel $Al_{0.3}Ga_{0.7}N$/ GaN HEMT, where L=1 μm is length of the gate metal as shown in Fig.1. The gate electrode is schottky barries placed on AlGaN cap layer of 3nm thickness.Cap layer is further placed over Si doped barrier layer of 18 nm thickness. A spacer layer of 3 nm thickness is used between top barrier layer and 14nm thick GaN channel layer in order to reduce impurity scattering. Gate is made of Ni-Au forming Schottky junction with semiconductor. This metal gate modulate the charge in the two conducting channels (top channel and bottom channel) formed at hetrointerface of $Al_{0.3}Ga_{0.7}N$ / GaN / $Al_mGa_{1-m}N$ / GaN epi-layers in the device. Undoped AlGaN spacer layer is introduced to reduce ionized scattering in the device. In the device structure the source and drain contact regions are uniformally doped as $N_d^+=10^{26}$ m^{-3} to make ohmic contacts. It is assumed that Si doped $Al_{0.3}$ $Ga_{0.7}$ N barrier layer is fully depleted under normal operating conditions and electons are confined in both the channels to the GaN side hetrointerface forming 2-DEG for each channel.

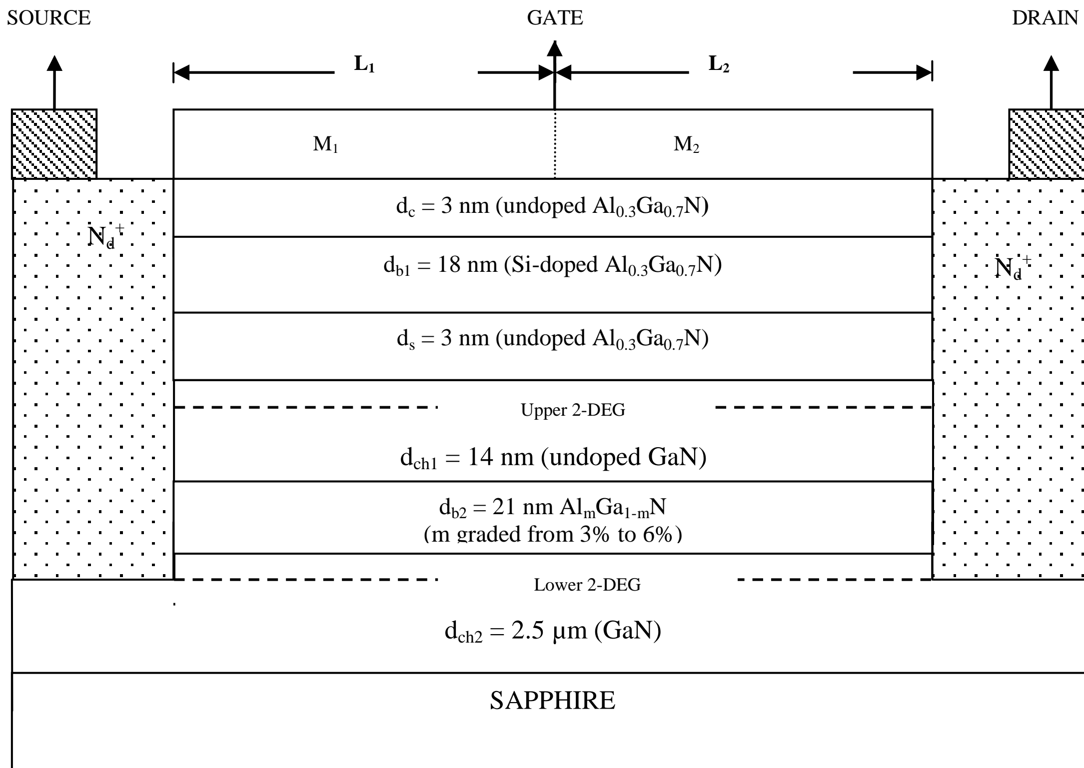

Fig.1. Cross sectional schematic of DCDMG AlGaN/GaN HEMT based on double channel AlGaN/GaN HEMT epilayer on sapphire substrate [6][19], Total gate length (L)=L_1+L_2, $L_1=L_2=0.5$μm, work function of gate region M_1 (ϕ_{M1}) =5.3V, work function of gate region M_2 (ϕ_{M2}) =4.1V [4][5], Gate width (W) =100**μ**m, $N_d=2\text{x}10^{24}m^{-3}$, $d_1=d_{b1}+d_s+d_c+\Delta d_1$ and $d_2=d_1+d_{ch1}+d_{b2}+\Delta d_2$ are distance of upper channel and lower channel from gate , Δd_1 and Δd_2 denotes 2DEG effective depth in upper and lowere GaN layers respectively.

For normally on device the Si-doped barrier layer is fully depleted without any gate bias and 2 DEG in each channel is available for current conduction. When an external bias is applied the n-$Al_mGa_{1-m}N$ barrier layer with Al mole fraction m=0.3 is depleted partially at the hetrointerface by the electron diffision into the channel and partially at the surface due to Schottky barrier [7-9]. For complete charge control by the gate the channel region must completely overlap to deplete the n-AlGaN layers so that only 2-DEG high mobility charge carriers take part in current conduction process in channels. Considering spontaneous and pizoelectric polarization at the hetrointerface the sheet carrier concentration of 2-DEG in upper channels is obtained [15] as

$$n_{s11}(m,x) = \frac{\epsilon(m)}{qd_1}\left(V_{gs} - V_{th1}(m) - V_{c11}(x)\right) \qquad for\ 0 \le x \le L_1 \tag{1}$$

$$n_{s12}(m,x) = \frac{\epsilon(m)}{qd_1}\left(V_{gs} - V_{th1}(m) - V_{c12}(x)\right) \qquad for L_1 \le x \le L_2 \tag{2}$$

With $\epsilon(m)$ as $Al_mGa_{1-m}N$ dielectric constant, and m=0.3 is Al mole fraction in it, $V_{c11}(x)$ and $V_{c12}(x)$ are upper channel potentials under gate regions M_1 and M_2 respectively at any point x along the regions, V_{gs} as gate to source bias, $d_1 = d_{b1} + d_s + d_c + \Delta d_1$ as separation between gate and upper channel and Δd_1 depth of 2DEG in upper GaN layer from its top edge.

Similarily, the sheet carrier concentration of 2-DEG in lower channels is obtained as

$$n_{s21}(m,x) = \frac{\epsilon(m)}{qd_2}\left(V_{gs} - V_{th2}(m) - V_{c21}(x)\right) \qquad for\ 0 \le x \le L_1 \tag{3}$$

$$n_{s22}(m,x) = \frac{\epsilon(m)}{qd_2}\left(V_{gs} - V_{th2}(m) - V_{c22}(x)\right) \qquad for\ L_1 \le x \le L_2 \tag{4}$$

Where $V_{c21}(x)$ and $V_{c22}(x)$ are lower channel potentials under gate regions M_1 and M_2 respectively at any point x along the regions. $d_2 = d_1 + d_{ch1} + d_{b2} + \Delta d_2$ is separation between gate and lower channel where Δd_2 is depth of 2DEG in lower GaN layer from its top edge.

The device threshold voltages is the gate to source voltage at which $V_{c11}(x)$ or $V_{c12}(x)$ becomes equal to double of flatband voltage and occurs under M_1 for upper and lower channels and obtained [10] as

$$V_{th11}(m) = \chi_1(m) - \Delta\varphi(m) - \frac{qN_d\, d_{b1}^2}{2\,\epsilon(m)} - \frac{\sigma_{pz}(m)d_1}{\epsilon(m)} \tag{5}$$

$$V_{th12}(m) = \chi_2(m) - \Delta\varphi(m) - \frac{qN_d\, d_{b1}^2}{2\,\epsilon(m)} - \frac{\sigma_{pz}(m)d_1}{\epsilon(m)} \tag{6}$$

$$V_{th21}(m) = \chi_1(m) - \Delta\varphi(m) - \frac{qN_d\, d_{b2}^2}{2\,\epsilon(m)} - \frac{\sigma_{pz}(m)d_2}{\epsilon(m)} \tag{7}$$

$$V_{th22}(m) = \chi_2(m) - \Delta\varphi(m) - \frac{qN_d\, d_{b2}^2}{2\,\epsilon(m)} - \frac{\sigma_{pz}(m)d_2}{\epsilon(m)} \tag{8}$$

where $\chi_1(m)$ and is $\chi_2(m)$ are the Schottky barrier height under M_1 and M_2 rsepectively, $\Delta\varphi(m)$ as the conduction band discontinuity at the $Al_mGa_{1-m}N$/GaN hetrointerface. N_d is Si doping concentration of n-AlGaN layer, $\sigma_{pz}(m)$ net polarization induced sheet carrier density at the hetrointerfaces and obtained as

$$\sigma_{pz}(m) = [\ P_{SP}(m) - P_{SP}(0) + P_{pz}\ ] \tag{9}$$

$\chi_1(m)$ is higher than $\chi_2(m)$ for Schottky junctions under M_1 and M_2 thus $V_{th11}(m)$ will be playing decisive role for upper channel current control. Similarily $V_{th21}(m)$ will be playing decisive role in controll of lower channel current.

Where $P_{SP}(m)$ and $P_{SP}(0)$ are spontaneous polarization of $Al_mGa_{1-m}N$ and GaN material system respectively [1][11][12].

In our model piezoelectric polarization depends on the amount of strain developed at hetrointerfaces in order to accommodate the difference in lattice constants of GaN and AlGaN. For fully satrained device piezoelectric polarization dependent charge density is given as

$$P_{pz} = 2\left(\frac{a(0)-a(m)}{a(m)}\right)\left(e_{31}(m) - e_{33}(m)\frac{C_{13}(m)}{C_{33}(m)}\right) \text{ for } 0 \le m \le 1$$

$$|\sigma_{pz}(m)| = \left|2\left(\frac{a(0)-a(m)}{a(m)}\right)\left(e_{31}(m) - e_{33}(m)\frac{C_{13}(m)}{C_{33}(m)}\right) + P_{SP}(m) - P_{SP}(0)\right| \quad \text{for } 0 \le m \le 1 \tag{10}$$

Whre $a(m)$ is lattice constant $e_{31}(m)$ and $e_{33}(m)$ are piezoelecric constants and $C_{13}(m)$ and $C_{33}(m)$ are elastic constants [12][13].

Increasing Al mole fraction in barrier layer increases lattice mismatch that further results in stain relaxation. For partially relaxed device with $Al_mGa_{1-m}N$ layer thickness in the range of 18nm to 40 nm piezoelectric polarization induced charge density depends on the Al mole fraction as [14].

$$P_{Pz} = \begin{cases} 2\left(\frac{a(0)-a(m)}{a(m)}\right)\left(e_{31}(m) - e_{33}(m)\frac{C_{13}(m)}{C_{33}(m)}\right) & for \quad 0 \le m \le 0.38 \\ 2\left(\frac{2.33-3.5\,m}{\frac{a(0)-a(m)}{a(m)}}\right)\left(e_{31}(m) - e_{33}(m)\frac{C_{13}(m)}{C_{33}(m)}\right) & for\ 0.38 \le m \le 0.67 \\ 0 & for\ 0.67 \le m \le 1 \end{cases} \tag{11}$$

In above equation (7) device remains completely strained for Al molefraction up to 38% and partially relaxed for m from 38% to 67%. Device is fully relaxed for m greater than 67%.

Table (A). List of material parameters of $Al_mGa_{1-m}N/GaN$ for m=0.30		
$a(0)$	lattice constant	3.1890 Ȧ
$a(m$	lattice constant	3.1659 Ȧ
$e_{31}(m)$	piezoelectric constant (x,y)	- 0.523C/m^2
$e_{33}(m)$	piezoelectric constant (z)	0.949 C/m^2
$C_{13}(m)$	elastic constant (x,y)	104.5 G Pa
$C_{33}(m)$	elastic constant (z)	395.4 G Pa
$P_{SP}(0)$	spontaneous polarization GaN	- 0.029 C/m^2
$P_{SP}(m)$	spontaneous polarization $Al_mGa_{1-m}N$	- 0.038 C/m^2

A. Current Voltage Characteristics Model:

Linear Region Model: Double channel device current can be obtained using current density equation for upper and lower channel as

$$I_{ds11}(m,x) = Zq\mu_1(x)\left(n_{s11}(m,x)\frac{dV_{c11}(x)}{dx} + \frac{kT}{q}\frac{dn_{s11}(m,x)}{dx}\right) \quad (12)$$

$$I_{ds12}(m,x) = Zq\mu_1(x)\left(n_{s12}(m,x)\frac{dV_{c12}(x)}{dx} + \frac{kT}{q}\frac{dn_{s1}(m,x)}{dx}\right) \quad (13)$$

$$I_{ds21}(m,x) = Zq\mu_2(x)\left(n_{s21}(m,x)\frac{dV_{c21}(x)}{dx} + \frac{kT}{q}\frac{dn_{s21}(m,x)}{dx}\right) \quad (14)$$

$$I_{ds22}(m,x) = Zq\mu_2(x)\left(n_{s22}(m,x)\frac{dV_{c22}(x)}{dx} + \frac{kT}{q}\frac{dn_{s}2(m,x)}{dx}\right) \quad (15)$$

where Z is gate width, $V_{c11}(x)$ and $V_{c12}(x)$ are channel potential in upper channel along x axis respectively under M_1 and M_2 respectively, $V_{c21}(x)$ and $V_{c22}(x)$ are channel potential in lower channel along x axis respectively under M_1 and M_2 regions, q is electron charge, k is Boltzmann constant, T is ambient temperature. The field dependent electron mobility in each channel is obtained [16][17] as

$$\mu_1(x) = \frac{\mu_0}{1+\left(\frac{\mu_0 E_{c1}-v_s}{E_{c1}v_s}\right)\frac{dV_{c1}(x)}{dx}} \quad (16)$$

$$\mu_2(x) = \frac{\mu_0}{1+\left(\frac{\mu_0 E_{c2}-v_s}{E_{c2}v_s}\right)\frac{dV_{c2}(x)}{dx}} \quad (17)$$

Where, μ_0 is low field mobility, E_{c1} , E_{c2} are critical electric fields for channels, and v_s is saturation drift velocities of the electrons in channels.

Using (1) and (16) in (12) we obtain

$$I_{ds11}(m,x)\left(1+\left(\frac{\mu_0 E_{c1}-v_s}{E_{c1}v_s}\right)\frac{dV_{c11}(x)}{dx}\right) = Z\mu_0\frac{\epsilon(m)}{d_1}\left((V_{eff11}(m) - V_{c11}(x))\frac{dV_{c11}(x)}{dx}\right) \quad (18)$$

$$I_{ds12}(m,x)\left(1+\left(\frac{\mu_0 E_{c1}-v_s}{E_{c1}v_s}\right)\frac{dV_{c12}(x)}{dx}\right) = Z\mu_0\frac{\epsilon(m)}{d_1}\left((V_{eff12}(m) - V_{c12}(x))\frac{dV_{c12}(x)}{dx}\right) \quad (19)$$

Similarly, using (2) and (17) in (14) we obtain

$$I_{ds21}(m,x)\left(1+\left(\frac{\mu_0 E_{c2}-v_s}{E_{c2}v_s}\right)\frac{dV_{c21}(x)}{dx}\right) = Z\mu_0\frac{\epsilon(m)}{d_2}\left((V_{eff21}(m) - V_{c21}(x))\frac{dV_{c21}(x)}{dx}\right) \quad (20)$$

$$I_{ds22}(m,x)\left(1+\left(\frac{\mu_0 E_{c2}-v_s}{E_{c2}v_s}\right)\frac{dV_{c22}(x)}{dx}\right) = Z\mu_0\frac{\epsilon(m)}{d_2}\left((V_{eff22}(m) - V_{c22}(x))\frac{dV_{c22}(x)}{dx}\right) \quad (21)$$

where

$$V_{eff11} = V_{gs} - V_{th11}(m) - \frac{kT}{q} \quad (22)$$

$$V_{eff12} = V_{gs} - V_{th12}(m) - \frac{kT}{q} \quad (23)$$

$$V_{eff21} = V_{gs} - V_{th21}(m) - \frac{kT}{q} \quad (24)$$

$$V_{eff22} = V_{gs} - V_{th22}(m) - \frac{kT}{q} \quad (25)$$

Among the upper channel series currents, $I_{ds11}(m)$ is more effective due to higher Schottky barrier height of gate region M_1. Now, integrating (18) and (20) with boundary conditions at $x = 0$

$$V_{c11}(x)|_{x=0} = I_{ds11}(m)R_s \quad (26)$$

For similar reasons, effective lower channel current is $I_{ds21}(m)$.

$$V_{c21}(x)|_{x=0} = I_{ds21}(m)R_s \quad (27)$$

By integrating (19) and (21) with boundary conditions at $x = L$, the drain side for upper channel

$$V_{c11}(x)|_{x=L} = V_{ds} - I_{ds11}(m)(R_s + R_d) \quad (28)$$

Similarly for lower channel

$$V_{c21}(x)|_{x=L} = V_{ds} - I_{ds21}(m)(R_s + R_d) \quad (29)$$

 © 2015, AIJRSTEM All Rights Reserved

Where, $L = L_1 + L_2$, is gate length, V_{ds} is applied drain bias, R_d and R_s are parasitic source and drain resistances respectively. The linear current equation for upper channel is obtained as

$$I_{ds11}(m) = \frac{-\alpha_2(m) \pm \sqrt{\alpha_2(m)^2 - 4\alpha_1(m)\alpha_3(m)}}{2\alpha_1(m)} \quad (30)$$

Where,

$$\alpha_1(m) = \left(\frac{\mu_0 E_{c1} - v_s}{E_{c1}\ v_s}\right)(2R_s + R_d) - \left(\frac{Z\mu_0 \epsilon(m}{2d_1}\right)(R_d^2 + 2R_sR_d) \quad (31)$$

$$\alpha_2(m) = \left(\frac{Z\mu_0 \epsilon(m}{d_1}\right)\left(V_{ds}(R_s + R_d) + V_{eff11}(m)(2R_s + R_d)\right) - L - V_{ds}\left(\frac{\mu_0 E_{c1} - v_s}{E_{c1}\ v_s}\right) \quad (32)$$

$$\alpha_3(m) = \left(\frac{Z\mu_0 \epsilon(m}{d_1}\right)\left(V_{eff11}(m)V_{ds} - \frac{V_{ds}^2}{2}\right) \quad (33)$$

Similarly,linear current equation for lower channel is given by

$$I_{ds21}(m) = \frac{-\beta_2(m) \pm \sqrt{\beta_2(m)^2 - 4\beta_1(m)\beta_3(m)}}{2\beta_1(m)} \quad (34)$$

Where,

$$\beta_1(m) = \left(\frac{\mu_0 E_{c2} - v_s}{E_{c2}\ v_s}\right)(2R_s + R_d) - \left(\frac{Z\mu_0 \epsilon(m}{2d_2}\right)(R_d^2 + 2R_sR_d) \quad (35)$$

$$\beta_2(m) = \left(\frac{Z\mu_0 \epsilon(m}{d_2}\right)\left(V_{ds}(R_s + R_d) + V_{eff21}(m)(2R_s + R_d)\right) - L - V_{ds}\left(\frac{\mu_0 E_{c2} - v_s}{E_{c2}\ v_s}\right) \quad (36)$$

$$\beta_3(m) = \left(\frac{Z\mu_0 \epsilon(m}{d_2}\right)\left(V_{eff21}(m)V_{ds} - \frac{V_{ds}^2}{2}\right) \quad (37)$$

Thus, device current for linear region is obtained by summation of both channel linear region currents, as

$$I_{dslin}(m) = I_{ds11}(m) + I_{ds21}(m) \quad (38)$$

***Saturation Region Mode*l:** In saturation region, at onset of saturation the potential in both the channels attains drain saturation voltage, $V_{dsat11}(m)$ and $V_{dsat21}(m)$ respectively. Similarly, electric field attains critical value E_{c1} and E_{c2} respectively. The current in saturation region in upper channel, I_{dsat11}can be obtained from equation (30) by substituting V_{ds} by $V_{dsat11}(m)$ obtained as

$$V_{dsat11}(m) = \frac{-\omega_2(m) \pm \sqrt{\omega_2(m)^2 - 4\omega_1(m)\omega_3(m)}}{2\omega_1(m)} \quad (39)$$

where

$$\omega_1(m) = \theta(m) + \left(\frac{Z\mu_0 \epsilon(m}{d_1}\right)\left(\left(\frac{\mu_0 E_{c1} - v_s}{E_{c1}\ v_s}\right) - \frac{1}{2}\right) - \left(\frac{Z\mu_0 \epsilon(m)}{d_1}\right)^2 E_{c1}(R_s + R_d) \quad (40)$$

$$\omega_2(m) = \left(\frac{Z\mu_0 \epsilon(m}{d_1}\right)\left(\frac{\mu_0 E_{c1} V_{eff11}(m)}{v_s} + E_{c1}L\right) - 2V_{eff11}(m)\theta(m) + \left(\frac{Z\mu_0 \epsilon(m)}{d_1}\right)^3 E_{c1}V_{eff11}(m)(3R_s + 2R_d) \quad (41)$$

(31)

$$\omega_3(m) = \theta(m)V_{eff11}^2(m) - \left(\frac{Z\mu_0 \epsilon(m}{d_1}\right)V_{eff11}(m)E_{c1}L - \left(\frac{Z\mu_0 \epsilon(m)}{d_1}\right)^3 V_{eff11}^2(m)E_{c1}(2R_s + R_d) \quad (42)$$

Where,

$$\theta(m) = \left(\frac{Z\mu_0 \epsilon(m)E_{c1}}{d_1}\right)^2\left(\frac{\mu_0 E_{c1} - v_s}{E_{c1}\ v_s}\right)(2R_s + R_d) - \left(\frac{Z\mu_0 \epsilon(m)}{d_1}\right)^3 \frac{{E_{c1}}^2}{2}(R_d^2 + 2R_sR_d) \quad (43)$$

Similarly, the current in saturation region in lower channel, I_{dsat21} can be obtained from (34) by substituting V_{ds} by $V_{dsat21}(m)$ obtained as

$$V_{dsat21}(m) = \frac{-\delta_2(m) \pm \sqrt{\delta_2(m)^2 - 4\delta_1(m)\delta_2(m)}}{2\delta_1(m)} \quad (44)$$

Where,

$$\delta_1(m) = \lambda(m) + \left(\frac{Z\mu_0 \epsilon(m)}{d_2}\right)\left(\left(\frac{\mu_0 E_{c2} - v_s}{E_{c2}\ v_s}\right) - \frac{1}{2}\right) - \left(\frac{Z\mu_0 \epsilon(m)}{d_2}\right)^2 E_{c2}(R_s + R_d) \quad (45)$$

$$\delta_2(m) = \left(\frac{Z\mu_0 \epsilon(m)}{d_2}\right)\left(\frac{\mu_0 E_{c2} V_{eff21}(m)}{v_s} + E_{c2}L\right) - 2V_{eff21}(m)\lambda(m) + \left(\frac{Z\mu_0 \epsilon(m)}{d_2}\right)^3 E_{c2}V_{eff21}(m)(3R_s + 2R_d) \quad (46)$$

(36)

$$\delta_3(m) = \lambda(m)V_{eff21}^2(m) - \left(\frac{Z\mu_0 \epsilon(m}{d_2}\right)V_{eff21}(m)E_{c2}L - \left(\frac{Z\mu_0 \epsilon(m)}{d_2}\right)^3 V_{eff21}^2(m)E_{c2}(2R_s + R_d) \quad (47)$$

Where,

$$\lambda(m) = \left(\frac{Z\mu_0 \epsilon(m)E_{c2}}{d_2}\right)^2\left(\frac{\mu_0 E_{c2} - v_s}{E_{c2}\ v_s}\right)(2R_s + R_d) - \left(\frac{Z\mu_0 \epsilon(m)}{d_2}\right)^3 \frac{{E_{c2}}^2}{2}(R_d^2 + 2R_sR_d) \quad (48)$$

Thus, device current in saturation region is obtained as

$$I_{dsat}(m) = I_{dsat11}(m) + I_{dsat21}(m) \quad (49)$$

III. Results and Discussion

To verify the present double channel dual material gate DCDMG AlGaN/GaN HEMT analytical DC model, the results obtained have been compared with experimental results [6]. Fig. 2 shows the cumulative drain current in both the channels as extracted from the analytical model, ATLAS simulation[20] and experimental data [6]. In this figure, the dash lines represent the model results while the solid lines display experimental data and triangular markers show simulated data for various gate to source bias. This figure clearly shows output characteristics of device in linear and saturation regions at gate to source voltages starts at 1.5V, 0V and -1 V. The drain current of the device is increasing from approximately 500 mA/mm to 1060 mA/mm with increasing gate to source bias. This results are in close agreement wih reported experimental data [6]. In our model, drain current is changing with the distance of the channels from the gate surface, depicting the current collapse in each channel is inversely proportional to the distance from the device gate. It was found that the current collapse mainly occuers in channel closer to the device surface, while the lower channel suffers minimal current collapse. The effect on drain current of distance of the channels from the the device surface is also depicted in our current-voltage model.

Fig.3 shows the input/ transfer characteristics of double channel dual material gate AlGaN/GaN HEMT depicting variation of drain current wih gate to source voltage at V_{ds} = 10 V with 1x 100 μm^2 device. This double channel AlGaN/GaN HEMT shows high current density with respect to conventional single channel AlGaN/GaN HEMT and also have good control of gate voltage on device drain current[18]. Our model results fit simulation and experimental data [6] reasonably well with a marginal discrepency at low gate biases. This may be attributed to minor gate and substrate leakage current that become more dominent, when the drain voltage becomes much higher then the effective gate voltage, therefore causing large electric fields at the drain end of the gate. Also, under the low gate biases the drain current of our model is little higher than the experimental data, which might be attributed to the error of the calculated threshold voltages. The reason can be that the approximation of the full depletion is introduced to obtain the threshold voltage, which assumes that there is no free charge in the spacer layer and that the doners in the n-AlGaN layer have been totally ionized. Thus we may interprete that there is no parasitric conduction path in Si doped n-AlGaN barrier layer due to thin width and Schottky and hetrojunction depletion regions are overlapping each other.

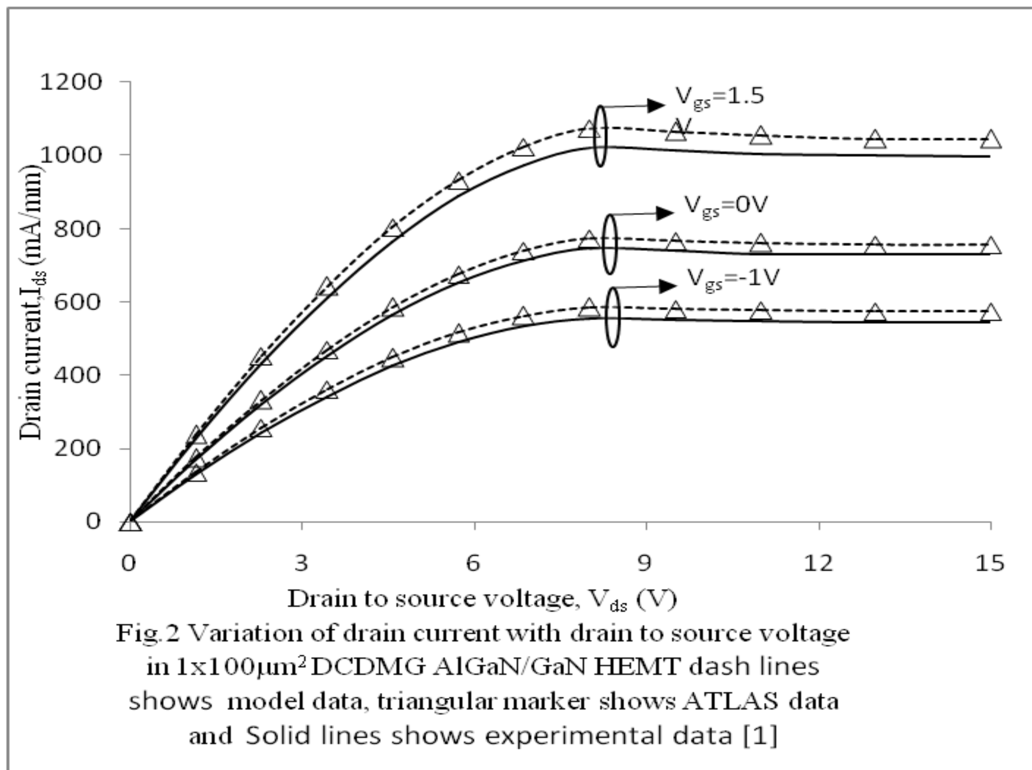

Fig.2 Variation of drain current with drain to source voltage in 1x100μm^2 DCDMG AlGaN/GaN HEMT dash lines shows model data, triangular marker shows ATLAS data and Solid lines shows experimental data [1]

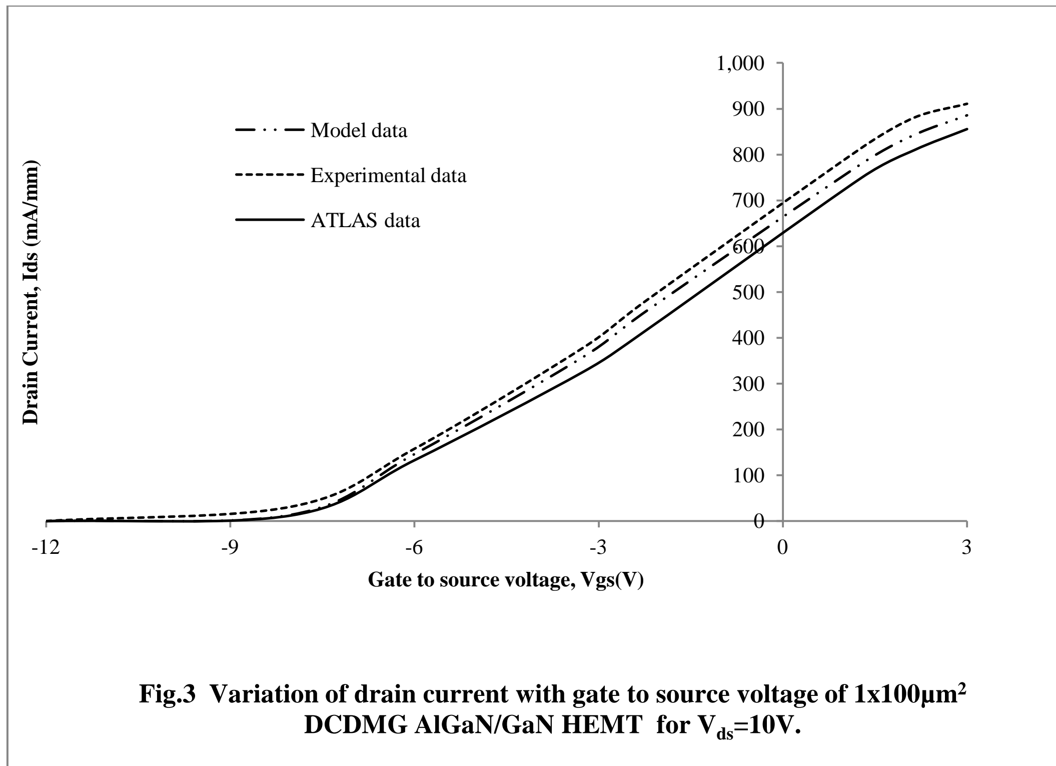

Fig.3 Variation of drain current with gate to source voltage of 1x100µm^2 DCDMG AlGaN/GaN HEMT for V_{ds}=10V.

IV. Conclusions

The dc large signal parameters of double channel dual material gate DCDMG Al_m $Ga_{1-m}N/GaN$ HEMT has been first time examined by developing 2-D analytical model. The expressions for both the top and bottom channel currents, have been obtained using semiconductor device physiscs. This model proves the superiority of double channel dual material gate Al_m $Ga_{1-m}N/GaN$ HEMT over conventional single channel AlGaN/GaN HEMTs in terms of high current drive capability and minimization of overall current collapse, due to introduction of lower channel which is at far distance than first channel from gate. The results obtained from our model agree well with the simulated and experimental results within the reasonable range of $\pm$ 5%.

It is evident from the resuls that DCDMG $Al_{0.3}Ga_{0.7}$ N/GaN HEMT introduces step functions in each channel potential profile thus, provide screening effects in small channel devices and suppressing short channel effects (SCE). The enhanced channel potential near source further results into more uniform average drift velocity of electrons in both the channels. This leads to improve carrier transport efficiency in the proposed device structure. Due to higher break down electric field capability of GaN material the proposed device is suitable for high power, high voltage and high speed microwave and radar applications.

Using further structure optimization techniques with the use of analytical expressions described in our proposed model, the improved double channel dual material gate AlGaN/GaN HEMTs with controlled 2-DEG carrier density under each gate region for the channels, higher efficiency microwave amplifiers, oscilators and analog frequency multipliers can be designed with more degree of freedom to engineer the gain linearity of the device.

References

[1] O. Ambacher, J. Smart, J. R. Shealy, N. G. Weimann, K. Chu, M.Murphy, W. J. Schaff, L. F. Eastman, R. Dimitrov, L. Wittmer, M. Stutzmann, W. Rieger, and J. Hilsenbeck, “Two-dimensional electron gases induced by spontaneous and piezoelectric polarization charges in N- and Ga-face AlGaN/GaN heterostructures”, J. Appl. Phys, vol. 85, no. 6, pp.3222–3233,Mar.1999.

[2] U. K. Mishra, P. Parikh, and Y. F. Wu, “AlGaN/GaN HEMTs—An Overview of Device Operation and Applications,” Proc. IEEE, vol. 90, no.6, pp. 1022–1031, Jun 2002.

[3] K.Kasahara, N. Miyamoto, Y. Ando, Y. Okamoto, T. Nakayama, and M.Kuzuhara, “Ka-band 2.3 W power AlGaN/GaN hetrojunction FET,” in IEDM Tech. Dig., pp. 667–680, Dec. 2002.

[4] W. Long, H. Ou, J. M. Kuo and K.K Chin., "Dual-Material Gate (DMG) Field Effect Transistor”, IEEE Trans. Electron Devices, vol. 46, pp. 865-870, May 1999.

[5] W. Long et.al. “Methods for fabricating a dual material gate of a short channel field effect transistor,” US Patent, US006153534, Nov 2000..

[6]] Roanming Chu,Yugang Zhou, Zie Liu, Deliang Wang, Kevin J. Chen, “AlGaN/GaN Double Channel HEMT,” IEEE Transaction on Electron Devices, vol.52, no.4, Apr. 2005.

[7] P.M. Soloman and H Morkov modulation doped GaAs/AlGa As hetrojunction field effect transistor (MODFETs), ultrahighspeed device for supercomputers, IEEE Trans Electron Devices ED-31 (1984),1015-1027.

[8] H. Morkov , H. Unlu and G.Ji, Principle of technology of MODFETs. Wiley, New York, 1991

[9] D. Delagebeaudeuf, NuyenT.Linh, “Metal-(n)AlGaAs/ GaAs Two Dimensional Electron Gas FET,” IEEE Trans Electron Devices, vol.ED-29, no.6, pp.955-960, Jun.1982.

[10] S.M. Zee,Physics of semiconductor devices, Wiley New York, 2nd Ed, 1981.

[11] E.S. Hellman, “The polarity of GaN: A critical review”, MRS Internet J. Nitride Semiconduct. Res. 3, vol. 11, pp. 1-11, 1998.

[12] Y.Zhang,I.P.Smorchkova, C.R.Elsass, S.Kellar, J.P.EIbbetson, S.Denbaars, U.K.Mishra ans J.Singh “ Charge control and mobility in AlGaN/ GaN Transistor:Experimental and theoretical studies” J.Appl, vol.87, no11, pp.7981-7987, 2000.

[13] T.Li,R.P.Joshi and C.Fazi “Montecarlo evaluation of degeneracy and interface roughness effects on electron transport in AlGaN/ GaN hetrostructures” J.Appl,Phys vol.88, no.2, pp.829-837,2000.

[14] O. Ambacher, B.Foutz J. Smart, J. R. Shealy, N. G. Weimann, K. Chu, M.Murphy, A.J. Sierakowski, W. J. Schaff, L. F. Eastman, R. Dimitrov, M. Stutzmann and A Mitchell “Two-dimensional electron gases induced by spontaneous and piezoelectric polarization in undoped and doped AlGaN/GaN heterostructures”, J. Appl. Phys, vol. 87, no. 1, pp.334–344, 2000.

[15] Rashmi, A.Agrawal, S.Sen, S.Halder, R.S.Gupta, “Analytical model for DC characteristics and small signal parameters of AlGaN/GaN Modulation Doped Field Effect Transistor for microwave applications”, Microwave and Optical Technology Lett, vol.27, pp. 413-418, 2000.

[16] P.P.Ruden, J.D.Albrcht, A.Sustandi, S.C.Binari, K.Ikkossi-Anastasiou, M.G.Ancona, R.L.Henery, D.D.koleske and A.E.Wikenden,” Extrinsic performance limitations of AlGaN/GaN heterostructure field effect transistor,” MRS Internet, J Nitride Semiconduct. Res., 4S1, G6.35, 1999.

[17] Rashmi, A. Kranti, S.Haldar, R.S.Gupta, “An accurate charge control model for spontaneous and piezoelectric polarization dependent two dimensional electron gas (2-DEG) sheet charge density of lattice mismatched AlGaN/GaN HEMTs” Solid State Electron, vol. 46, no. 5, pp. 621-630, 2002.

[18] Y.F.Wu, B.P.Kellar, P.Fini, S.Kellar, T.J.Jenkins, L.T.Kehias, S.P.Denbaares and U.K.Mishra, “Bias dependent microwave performance of AlGaN/GaN MODFETs up to 100V,” IEEE Electron Device Lett.,vol.18, no.6, pp.290-292, Jun1997.

[19] Rahis Kumar Yadav, Pankaj Pathak, R M Mehra, “Analytical Modeling of Potential and Electric Field Distribution and Simulation of Large Signal Parameters for Dual Channel Dual Material Gate AlGaN/GaN High Electron Mobility Transistor.” International Journal of Research and Scientific Innovation, vol.2, issue.5, pp.49-55, May 2015.

[20] Silvaco TCAD, ATLAS Device Simulator. www.silvaco.com